J. Fluid Mech. (1984), *vol.* 149, *pp.* 127–146
Printed in Great Britain

Aerodynamic coefficients and longitudinal stability of sail aerofoils

By A. D. SNEYD
University of Waikato, Private Bag, Hamilton, New Zealand

This paper extends previous theoretical work on inextensible sails in two ways. First, the asymptotic expansion of sail camber in terms of the small angle of attack α is continued to include terms of order α^3, because only at this order can one obtain information about the longitudinal static stability of a sail aerofoil. Secondly, to describe aerofoils such as those found in pterodactyl or bat wings, we also consider pretensioned membranes which acquire camber by stretching the surface material, or bending the supporting structure. Approximate formulae are derived for the aerodynamic coefficients in the limits of large and small tension, and the effect of sail and structural flexibility on these coefficients is discussed.

1. Introduction

Several authors have studied two-dimensional irrotational inviscid flow over sails which are fixed at the leading and trailing edges. Thwaites (1961) and Nielsen (1963) solved this problem numerically, assuming that the angle of attack α were small, and using thin-aerofoil theory to obtain the first-order term in an asymptotic expansion. For finite α, Vanden-Broeck & Keller (1981) obtained approximate analytic solutions assuming high sail tension, while Bundock (1980) and Vanden-Broeck (1982) developed exact numerical methods. Except for Bundock, these authors have been concerned with inextensible sails, which can billow because they are slack, as is the case with yacht sails or hang-glider wings. In this paper we also consider aerofoil sections like those found in pterodactyl or bat wings, which consist of a stretched membrane and behave essentially like sails, but without slack, camber being accommodated by stretch in the membrane or bending of the supporting structure. Bundock (1980) studied a model sail which had constant tension, independent of its camber or the airflow. This represents the opposite extreme from the inextensible sail – the perfectly extensible sail. Stretched membrane aerofoils lie between these two extremes, and tension increases as the airflow stretches the material. Previous authors have usually given results for only the sail profile and lift coefficient, but this paper is particularly concerned with sail aerofoils in flight, so the moment coefficient and centre of pressure are equally important.

One difficulty with considering inextensible sails is that only in two-dimensional geometry – the sail of infinite span attached to fixed parallel leading and trailing edges – can changes in surface shape occur. In practice yacht sails are cut to assume a predetermined cambered shape and, if the sailcloth were inextensible, the first fundamental surface form (or metric tensor) would be fixed at manufacture. It is shown in Appendix A that, if the first fundamental form of a surface is given, and if two intersecting curves on the surface are also specified, then at least some part of the surface is uniquely determined. For example, the shape of an inextensible yacht sail would be completely determined by its cut, and by the shape of mast and boom

to which it were rigidly attached. Thus the camber of a two-dimensional sail can respond to aerodynamic forces in a way that is impossible for any finite inextensible sail, and a *rigid* surface might be a better model for three-dimensional problems. Real sailcloth is not quite inextensible (though this is considered a desirable ideal) and a realistic problem would involve the shape, airflow and tension distribution all as interrelated variables.

Section 2 of this paper describes the mathematical technique used to analyse the flow over a sail of given tension. The methods are similar to those of Nielsen (1963) – thin-aerofoil theory is used, but the small-α expansion is continued to include terms of order α^3. This is necessary because the $O(\alpha)$ expansion predicts the position of the centre of pressure of a sail without slack to be independent of α, which represents neutral longitudinal static stability. To obtain information about the movement of the centre of pressure with α, higher-order terms must therefore be included. The asymptotic expansion method is used in preference to the exact methods of Bundock (1980) or Vanden-Broeck (1982), because the $O(\alpha^3)$ terms show explicitly the form of the inaccuracy involved in linear theory. Also, if the expansion is truncated at $O(\alpha^3)$ one can describe static stability in terms of analytic formulae, such as (4.6), whereas the corresponding exact relation would have to be presented in graphic or tabular form.

It should be emphasized that these calculations in no way depend upon the sail material (so long as it is non-porous). The tension–elongation law for the material serves to determine the value of the tension in any particular application.

Section 3 discusses the results of the calculations and derives approximate formulae for the sail profile and aerodynamic coefficients in the limit as sail tension tends to its minimum possible value. The methods of Vanden-Broeck & Keller (1981) can be used to find similar approximations in the opposite limit of large tension, and comparison with exact results shows that one or other of the approximate formulae will always be reasonably accurate.

Section 4 applies the results of §3 to stretched-membrane sails whose tension varies linearly with sail extension. Since changes in sail length are of order the camber squared, the tension varies only slightly from its static value, and only the higher-order terms in the various aerodynamic coefficients are affected. Perfectly extensible (or constant-tension) sails are always statically stable, but this stability is lost for sails less easily stretched. All movements of the centre of pressure are $O(\alpha^2)$, whereas for rigid aerofoils they are $O(\alpha)$, and usually towards the leading edge as α increases, giving static instability. This is why rigid-winged aircraft need a secondary wing or tailplane to achieve static stability, whereas pterodactyls and bats may not.

Structural flexibility is most important at the trailing edge. For example, the leading edge of a hang-glider wing is usually a tubular aluminium spar, whereas the trailing edge consists of a tensioned wire, and it seems generally true for sail or membrane wings that the leading edge is more rigidly built. Section 4 therefore considers trailing-edge movement only, the main effect of which is to counteract any increase in α.

Sails with slack are considered in §5. These behave more like rigid aerofoils in that they retain finite camber as $\alpha \to 0$, and are statically unstable.

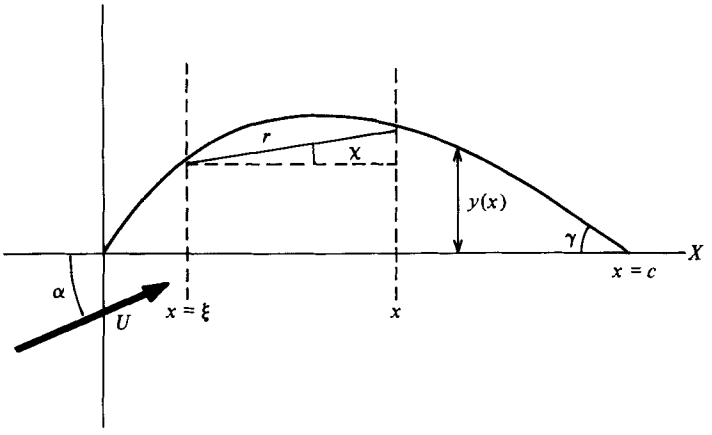

FIGURE 1. Diagram of sail.

2. Mathematical methods for a constant-tension sail

Airflow calculation for a given camber y(x)

The aerofoil to be analysed consists of an infinitely long strip of sail stretched at constant tension T (independent of length) between the leading edge $x = 0$ and trailing edge $x = c$, as shown in figure 1. The idea of a constant-tension or perfectly extensible sail is unphysical, but it is convenient to derive basic results for this simple situation, which can then be applied to more realistic sails. The airflow is assumed irrotational and incompressible, so that

$$\boldsymbol{u} = U(\cos\alpha + u)\,\hat{\boldsymbol{x}} + U(\sin\alpha + v)\,\hat{\boldsymbol{y}},$$

where the perturbation flow (u, v) is due to the presence of a vortex sheet on the sail surface, of strength $\omega(x)$ per unit length along the x-axis. The Kutta trailing-edge condition implies that

$$\omega(c) = 0. \tag{2.1}$$

The analytic function $u - \mathrm{i}v$ of $z = x + \mathrm{i}y$ is given by

$$u - \mathrm{i}v = \frac{\mathrm{i}}{2\pi}\int_0^c \frac{\omega(\xi)}{\xi + \mathrm{i}y(\xi) - z}\,\mathrm{d}\xi,$$

so one can apply the Plemelj formulae to find the mean perturbation components

$$\bar{u}_{\mathrm{s}} = \tfrac{1}{2}(u_{\mathrm{s}+} + u_{\mathrm{s}-}) = \frac{1}{2\pi}\int_0^c r^{-2}\omega(\xi)\,[y(\xi) - y(x)]\,\mathrm{d}\xi, \tag{2.2}$$

$$\bar{v}_{\mathrm{s}} = \tfrac{1}{2}(v_{\mathrm{s}+} + v_{\mathrm{s}-}) = \frac{1}{2\pi}\int_0^c r^{-2}\omega(\xi)\,(x - \xi)\,\mathrm{d}\xi, \tag{2.3}$$

where the subscripts s+, s− denote values of the variable on the upper and lower sail surfaces, and r is defined in figure 1. The Cauchy principal value of the singular integrals in (2.2) and (2.3) is to be understood, here and in the equations following.

The flow must be tangential to the sail surface, so

$$\sin\alpha + \bar{v}_{\mathrm{s}} = y'(x)\,(\bar{u}_{\mathrm{s}} + \cos\alpha). \tag{2.4}$$

The angle of attack α will be assumed small (as it must be in practice to avoid separation) and clearly $y(x)$ and $\omega(x)$ are odd functions of α, so one can write

$$y = \alpha y_1 + \alpha^3 y_3 + \ldots, \quad \omega = \alpha\omega_1 + \alpha^3\omega_3 + \ldots. \tag{2.5}$$

Substitution of (2.2) and (2.3) into (2.4) and equating terms of order α and order α^3 gives the following two integral equations for $\omega_1(x)$ and $\omega_3(x)$:

$$\frac{1}{2\pi}\int_0^c \frac{\omega_1(\xi)}{x-\xi}\,\mathrm{d}\xi = y_1'(x) - 1, \tag{2.6}$$

$$\frac{1}{2\pi}\int_0^c \frac{\omega_3(\xi)}{x-\xi}\,\mathrm{d}\xi = y_3'(x) + g(x), \tag{2.7}$$

where $g(x)$ depends on $y_1(x)$ and $\omega_1(x)$ and is given explicitly by (2.16).

Sail equilibrium equations

The pressure difference across the sail is balanced by tension, so using Bernoulli's theorem one obtains

$$\tfrac{1}{2}\rho(q_+^2 - q_-^2) = \kappa T, \tag{2.8}$$

where ρ is air density, κ is the sail curvature and q_+, q_- the flow speeds on the upper and lower surfaces. Equation (2.8) can be written:

$$-\rho U^2\omega_l\bar{q} = \kappa T,$$

where $U\omega_l = q_- - q_+$ is the vortex sheet strength per unit length along the sail, and $U\bar{q} = \tfrac{1}{2}(q_+ + q_-)$ is the average surface flow speed. Now $\omega_l = (\mathrm{d}x/\mathrm{d}l)\,\omega$ (l = arc-length along the sail surface) and $\bar{q} = (\cos\alpha + \bar{u}_s)\,\mathrm{d}l/\mathrm{d}x$, so

$$2\omega(\cos\alpha + \bar{u}_s) = cky''(1+y'^2)^{-\frac{3}{2}}, \tag{2.9}$$

where

$$k = T/(\tfrac{1}{2}\rho U^2 c)$$

is a dimensionless sail-tension coefficient. The $O(\alpha)$ and $O(\alpha^3)$ terms of (2.9) now give

$$\omega_1 = \tfrac{1}{2}cky_1'', \quad \omega_3 = \tfrac{1}{2}cky_3'' + h(x), \tag{2.10), (2.11}$$

where $h(x)$ includes nonlinear interactions of y_1 and ω_1 and the curvature correction, and is given explicitly by (2.17). Equations (2.6) and (2.10) can be solved to determine $y_1(x)$ and $\omega_1(x)$; then $h(x)$ and $g(x)$ are calculated and finally (2.7) and (2.11) solved to determine $y_3(x)$ and $\omega_3(x)$.

Numerical methods

The numerical method used is essentially that of Nielsen (1963). Under the substitutions

$$x = \tfrac{1}{2}c(1+\cos\theta), \quad \xi = \tfrac{1}{2}c(1+\cos\phi), \quad y_1'(x) = f_1(\theta), \quad y_3'(x) = f_3(\theta),$$

(2.6), (2.10), (2.7) and (2.11) become respectively

$$\frac{1}{2\pi}\int_0^\pi \frac{\omega_1(\phi)\sin\phi}{\cos\theta - \cos\phi}\,\mathrm{d}\phi = f_1(\theta) - 1, \tag{2.12}$$

$$\sin\theta\,\omega_1(\theta) = -k\frac{\mathrm{d}f_1}{\mathrm{d}\theta}, \tag{2.13}$$

$$\frac{1}{2\pi}\int_0^\pi \frac{\omega_3(\phi)\sin\phi}{\cos\theta - \cos\phi}\,\mathrm{d}\phi = f_3(\theta) + g(\theta), \tag{2.14}$$

$$\sin\theta\,\omega_3(\theta) = -k\frac{\mathrm{d}f_3}{\mathrm{d}\theta} + h(\theta), \tag{2.15}$$

where

$$g(\theta) = \frac{1}{6} + \frac{1}{2\pi}\int_0^\pi \frac{\omega_1(\phi)\tan^2\chi_1 \sin\phi}{\cos\theta - \cos\phi}\,\mathrm{d}\phi - \tfrac{1}{2}f_1(\theta) - \frac{f_1(\theta)}{2\pi}\int_0^\pi \frac{\omega_1(\phi)\tan\chi_1 \sin\phi}{\cos\theta - \cos\phi}\,\mathrm{d}\phi, \tag{2.16}$$

and

$$h(\theta) = \tfrac{1}{2}\omega_1(\theta)\sin\theta - \frac{\omega_1(\theta)\sin\theta}{2\pi}\int_0^\pi \frac{\omega_1(\phi)\tan\chi_1 \sin\phi}{\cos\theta - \cos\phi}\,\mathrm{d}\phi + \tfrac{3}{2}k_0\frac{\mathrm{d}f_1}{\mathrm{d}\theta}f_1^2(\theta). \tag{2.17}$$

The angle χ is shown in figure 1 and

$$\chi_1 = \arctan\frac{y_1(x) - y_1(\xi)}{x - \xi}.$$

The sail slope $f_1(\theta)$ is approximated by a cosine series,

$$f_1(\theta) = \sum_{n=0}^{N} \beta_n \cos n\theta, \tag{2.18}$$

and, since $y = 0$ at both leading and trailing edges,

$$\int_0^c y_1'(x)\,\mathrm{d}x = \tfrac{1}{2}c\int_0^\pi f_1(\theta)\sin\theta\,\mathrm{d}\theta = 0,$$

which gives

$$\beta_0 = \sum_{n=1}^{[\frac{1}{2}N]} \frac{\beta_{2n}}{4n^2 - 1}. \tag{2.19}$$

The usual methods of thin-aerofoil theory give the solution of (2.1) and (2.12) as

$$\omega_1(\theta) = 2(\beta_0 - 1)\frac{1 - \cos\theta}{\sin\theta} + 2\sum_{n=1}^{N} \beta_n \sin n\theta. \tag{2.20}$$

Expressions (2.18) and (2.20) are then substituted into (2.13) and the cosine functions on the left-hand side are expanded as sine series, using the formula

$$\cos n\theta = \sum_{p=1}^{\infty} a_{np} \sin p\theta \quad (0 \leqslant \theta \leqslant \pi),$$

where $a_{np} = 4p/\pi(p^2 - n^2)$ if $n + p$ is odd, and zero otherwise. Then equating the coefficients of $\sin n\theta$, $n = 1, 2, \ldots, N$, on each side, and applying (2.19) gives a system of $N + 1$ linear equations for $\beta_0, \ldots, \beta_N$. After some rather lengthy algebra, $g(\theta)$ can be determined in the form of a cosine series in θ, and $h(\theta)$ in the form of a sine series; then (2.14) and (2.15) are solved for $f_3(\theta)$ and $\omega_3(\theta)$ as before.

The equations for the β_i can be written

$$\sum_{j=0}^{N} A_{ij}\beta_j = c_i, \tag{2.21}$$

where

$$A_{ij} = ik\,\delta_{ij} + a_{j+1,\,i} - a_{j-1,\,i} \quad (i, j > 0);$$

$$A_{i0} = \begin{cases} 8i/\pi(i^2 - 1) & (i > 0 \text{ and even}), \\ 8/\pi i & (i \text{ odd}); \end{cases}$$

$$A_{00} = 1,$$

$$A_{0j} = \begin{cases} -1/(j^2 - 1) & (j \text{ even}), \\ 0 & (j \text{ odd}); \end{cases}$$

$$c_0 = 0, \quad c_i = -h_i + \sum_{j=0}^{N} g_j(a_{j-1,\,i} - a_{j+1,\,i}) \quad (i > 0).$$

N	10	16	20
$y_1(0.4)$	0.4292	0.4292	0.4291
$y_3(0.4)$	0.8153	0.8137	0.8134
C_{L1}	11.03	11.03	11.03
C_{L3}	3.744	3.712	3.714
C_{M1}	3.865	3.865	3.865
C_{M3}	2.001	1.983	1.984

TABLE 1. Convergence as $N \to \infty$ ($k = 3$)

The vectors g_i, h_i consist of the coefficients in the Fourier expansions of the forcing terms in (2.12)–(2.15). When solving for y_1, $g_0 = -1.0$ and the rest of the coefficients are zero; for y_3 the coefficients are found from (2.16) and (2.17).

Program checking

The computer program was written in Fortran 77 and the calculations performed on the University of Waikato Vax 11/780 computer. The aerodynamic section of the program was checked by comparison with the analytic solution for an aerofoil in the shape of a circular arc. The results for $y_1(x)$ and $\omega_1(x)$ were checked against Nielsen's (1963) results, and all results were checked for convergence as $k \to \infty$ to the analytic solution of Vanden-Broeck & Keller (1981). Finally convergence as $N \to \infty$ was checked by a comparison of results for various values of N, as shown in table 1.

3. Numerical results and asymptotic expansions

One important prediction of linear theory is that a minimum value of the sail-tension coefficient k, say k_c, is necessary to give a purely convex sail shape. As $k \to k_c$ from above, the camber function $y_1(x) \to \infty$, tension being insufficient to withstand the aerodynamic forces. The best estimate of k_c has been given by Chalmers (1966):

$$k_c = 1.7272.$$

The exact calculations of Bundock (1980) confirmed this singular behaviour at a certain k-value, $k_s(\alpha)$, which increased with α. In the limit $\alpha \to 0$, of course $k_s(\alpha) \to k_c$. Thwaites (1961) reported solutions of the sail equations for $k < k_c$ in which $y(x)$ is negative ('reverse-camber' solutions) or changes sign, and Haselgrove & Tuck (1976) analysed the profile stability of all solutions for inextensible sails. Except under certain carefully controlled conditions, profiles with $k < k_c$ are unstable, so the present calculations are generally restricted to $k > k_c$.

As $k \to k_c$ the lowest eigenvalue of the matrix $\boldsymbol{A}$ in (2.21) tends to zero, and it is shown in Appendix B that we can write

$$y_1(x) = (k-k_c)^{-1} F(x) + G(x) + O(k-k_c), \tag{3.1}$$

where the functions F, G, shown in figure 2, are independent of k. The function $F(x)$ corresponds to the zero eigenvector of $\boldsymbol{A}$ when $k = k_c$ and is symmetric. As k increases and contributions from G become more significant, the point of maximum camber moves towards the leading edge and the sail assumes its characteristic asymmetric shape. As $k \to \infty$ the point of maximum camber $\to x = 0.403c$. The higher-order camber functions $y_3(x)$, $y_5(x)$ etc. will have progressively stronger singularities as $k \to k_c$. Equations (2.16) and (2.17) show that, for the purposes of calculating y_3, the

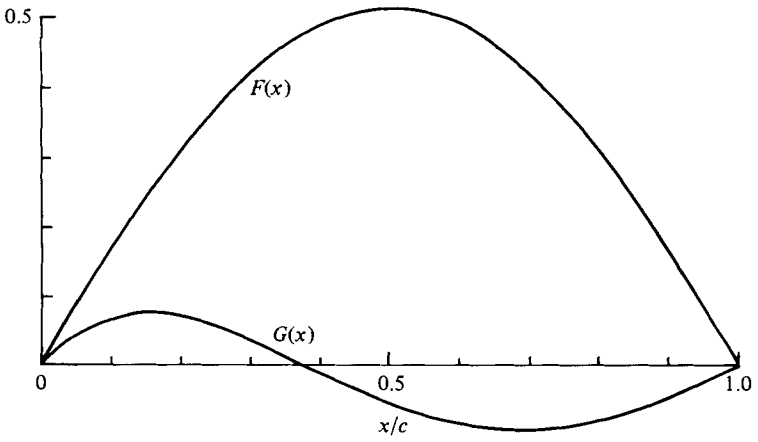

FIGURE 2. Graphs of $F(x)$ and $G(x)$.

vector c_i on the right-hand side of (2.21) will be of order $(k-k_c)^{-3}$ as $k \to k_c$. The singularity in $\boldsymbol{A}$ will provide a further factor of $(k-k_c)^{-1}$, so that altogether

$$y_3 = O(k-k_c)^{-4} \quad \text{as} \quad k \to k_c.$$

In general one would expect

$$y_{2n-1} = O(k-k_c)^{-(3n-2)},$$

so the condition for the convergence of (2.5) would be:

$$k-k_c > \text{constant} \times \alpha^{\frac{2}{3}},$$

or equivalently

$$k_s(\alpha) = k_c + \text{constant} \times \alpha^{\frac{2}{3}}.$$

This formula agrees with the results of Bundock (1980) in that k_s is an increasing function of α, but the above power law is inconsistent with his numerically calculated graph of $k_s(\alpha)$ against α.

Sail profiles

Graphs of $y_1(x)$ have been given by a number of authors, and are not repeated here, but figure 3 shows graphs of $y_3(x)$ for various values of k. The $O(\alpha)$ equations of thin-aerofoil theory tend to (i) overestimate the restoring force due to tension, and (ii) overestimate the aerodynamic forces (α instead of $\sin\alpha$). For small k and highly cambered sails effect (i) is predominant and the sail camber is underestimated, so that $y_3(x)$ is everywhere positive. Conversely for large k when the sail camber is small, it is overestimated and $y_3(x)$ is everywhere negative. For moderate values of k, $y_3(x)$ changes sign.

Lift and moment coefficients

Lift and moment coefficients C_L, C_M are defined by setting

$$C_L = \frac{L}{\frac{1}{2}\rho U^2 c}, \quad C_M = \frac{M}{\frac{1}{2}\rho U^2 c^2},$$

where L is the lift and M the moment of the aerodynamic forces about the leading

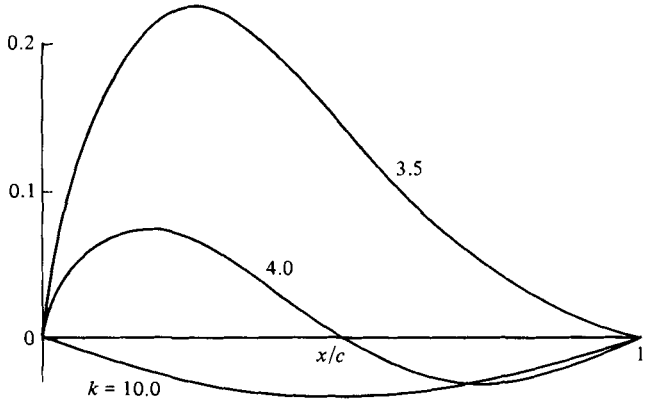

FIGURE 3. Graphs of $y_3(x)$.

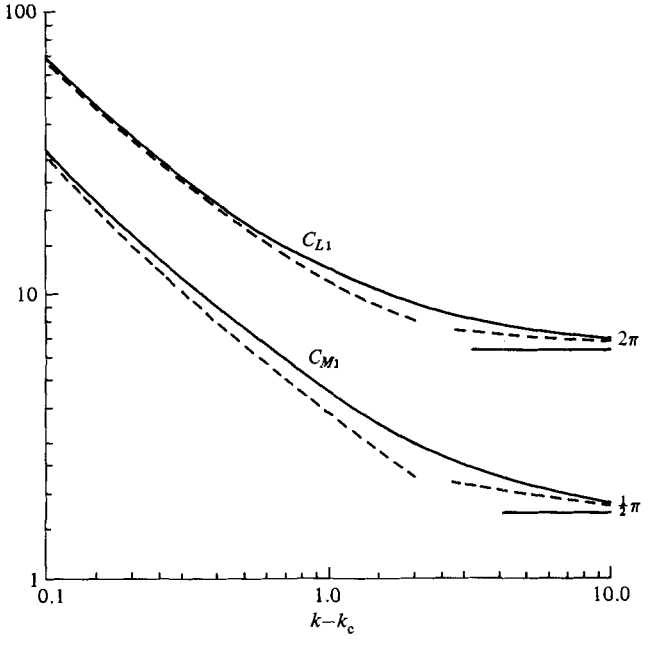

FIGURE 4. Graphs of C_{L1} and C_{M1} against k. The dashed lines represent the relevant approximation.

edge. These coefficients, like $y(x)$, are odd functions of α and can be expanded in the form

$$C_L = \alpha C_{L1} + \alpha^3 C_{L3} + \ldots, \tag{3.2}$$

$$C_M = \alpha C_{M1} + \alpha^3 C_{M3} + \ldots. \tag{3.3}$$

Figures 4 and 5 show graphs of C_{L1}, C_{L3}, C_{M1} and C_{M3} against k. The coefficients C_{L1} and C_{M1} increase with decreasing k because, as sail tension decreases, camber can increase more rapidly with α. Looking at (3.1) one can see that C_{L1} must have an asymptotic form

$$C_{L1} = (k-k_c)^{-1} C_{L11} + C_{L10} + O(k-k_c) \quad \text{as} \quad k \to k_c,$$

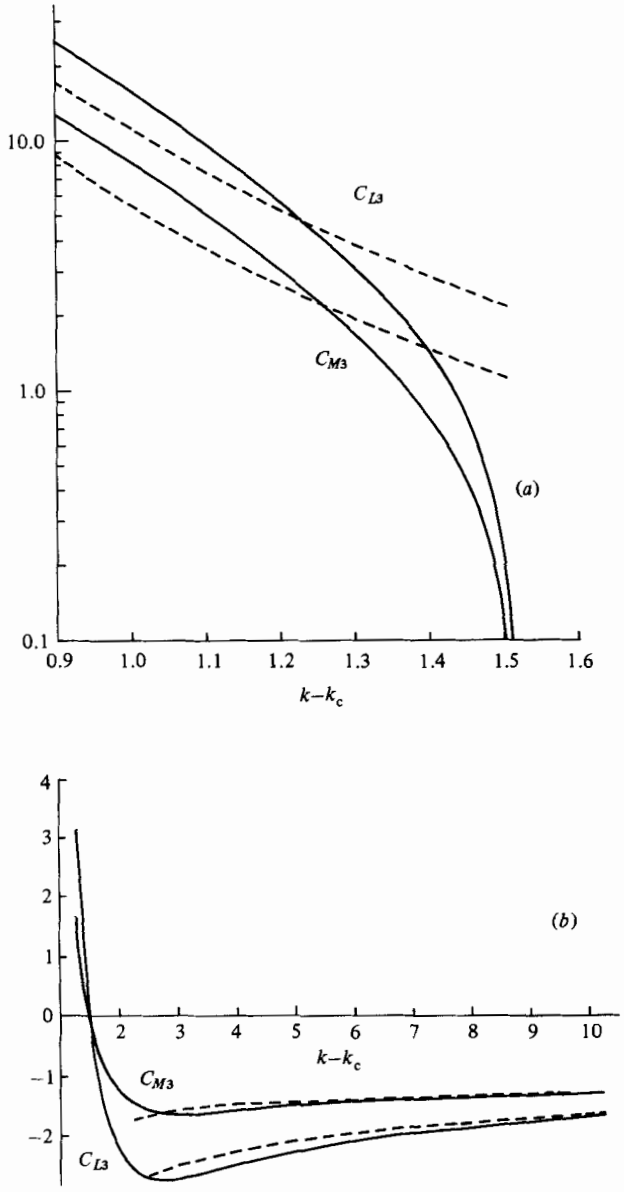

FIGURE 5. Graphs of C_{L3} and C_{M3} against k. The dashed lines represent the relevant approximation. Note that in (*a*) the coefficient scale is logarithmic.

and C_{M1} similarly. These expansions are summarized in table 2 and, for comparison, they are also graphed in figure 4. Similarly we expect C_{L3} to have an asymptotic form

$$C_{L3} = \sum_{n=0}^{4} C_{L3n}(k-k_c)^{-n} + O(k-k_c) \quad \text{as} \quad k \to k_c,$$

and also C_{M3}. Only the leading coefficient has been calculated, and the corresponding asymptotic formula is graphed in figure 5(*a*). A comparison for $k-k_c < 0.9$ was not possible because of convergence difficulties with the computer program. Figure 5(*b*)

Variable	$k\to\infty$	$k-k_c=t\to 0$
$y_1'(x)$	$2[\theta-\frac{1}{4}\pi-\sin\theta]$	$F'(x)\,t^{-1}+G'(x)$
C_{L1}	$2\pi+k^{-1}(16-\pi^2)$	$5.9691t^{-1}+5.1831$
C_{M1}	$\frac{1}{2}\pi+(1/12k)\,(64-3\pi^2)$	$2.9845t^{-1}+0.8639$
x_{p0}	$\frac{1}{4}+2/(3\pi k)$	$\frac{1}{2}-0.2894t$
C_{L3}	$-\frac{1}{3}\pi-(1/6k)\,(112-7\pi^2)$	$11.2532t^{-4}$
C_{M3}	$-\frac{1}{3}\pi-(1/18k)\,(256-21\pi^2)$	$5.6266t^{-4}$
x_{p2}	$(1/24\pi k)\,(9\pi^2-80)$	—
γ_1	$\pi/2k$	$1.7283t^{-1}-0.5052$
Δl	$(1/24k^2)\,(9\pi^2-64)$	$0.6718t^{-2}-0.0859t^{-1}$

TABLE 2. Asymptotic forms of aerodynamic coefficients etc.

shows graphs of C_{L3} and C_{M3} for larger values of k, and the behaviour as k increases reflects that of y_3.

Vanden-Broeck & Keller (1981) give the following approximation to the lift coefficient in the limit $k\to\infty$:

$$C_L = 2\pi\sin\alpha+\tfrac{1}{2}k^{-1}(16-\pi^2)\cos\alpha\sin 2\alpha+O(k^{-2}), \tag{3.4}$$

and an extension of their methods gives

$$C_M = \tfrac{1}{4}\pi\sin 2\alpha+k^{-1}\sin 2\alpha\,[\cos^2\alpha(\tfrac{8}{3}-\tfrac{1}{8}\pi^2)+\sin^2\alpha(\tfrac{3}{8}\pi^2-\tfrac{8}{3})]+O(k^{-2}). \tag{3.5}$$

From (3.4) and (3.5) one can derive large-k approximations for $C_{L1}, C_{M1}, C_{L3}, C_{M3}$, which are summarized in table 2. For comparison, graphs of these approximations are also shown in figures 4 and 5(*b*).

Longitudinal static stability

The line of action of the resultant of the aerodynamic forces acting on the aerofoil intersects the x-axis at the point cx_p, where

$$x_p = \frac{C_M}{C_L\cos\alpha}. \tag{3.6}$$

It follows from (3.2) and (3.3) that x_p can be expanded in the form:

$$x_p = x_{p0}+\alpha^2 x_{p2}+\ldots, \tag{3.7}$$

so that, to leading order, x_p is independent of α.

The sign of $\mathrm{d}x_p/\mathrm{d}\alpha$ determines the longitudinal static stability of the aerofoil. If this is positive, then any increase in α (say due to an upward gust) moves x_p towards the trailing edge and provides a moment tending to rotate the aerofoil leading edge downwards, and to restore the original value of α. This situation represents static stability, and conversely, if the sign is negative, we have instability. Equation (3.7) shows that to leading order, sail aerofoils have *neutral* static stability (Sneyd, Bundock & Reid 1982), in marked contrast with rigid aerofoils, which are generally unstable, the reason being as follows.

A rigid aerofoil has an aerodynamic centre – a point about which the pitching

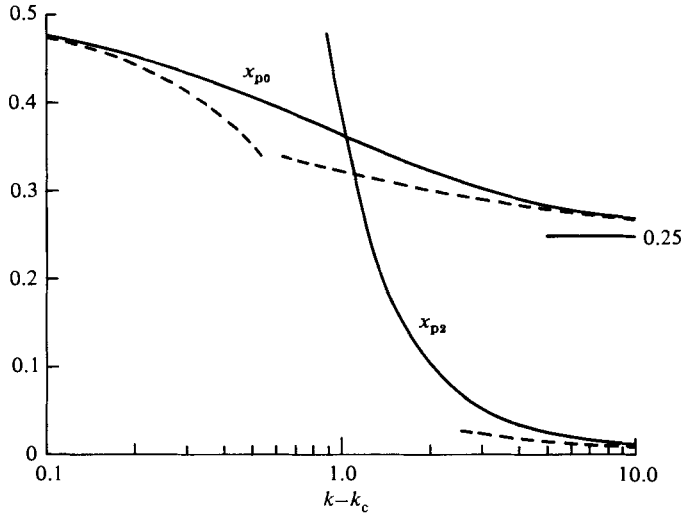

FIGURE 6. Graphs of x_{p0} and x_{p2} against k. The dashed lines represent the relevant approximation.

moment is independent of α – which for a thin aerofoil is approximately at the quarter-chord position, $x = \frac{1}{4}c$, $y = 0$. Thus

$$x_p = \tfrac{1}{4} + \frac{\bar{C}_M}{C_L},$$

where $\bar{C}_M$, the moment coefficient about the quarter-chord position, is constant. For aerofoils with positive camber everywhere, $\bar{C}_M$ is positive, and since C_L increases with α, $\mathrm{d}x_p/\mathrm{d}\alpha$ is negative. A constant-tension sail, on the other hand, does not have a fixed shape, its camber being approximately proportional to α. This means that there is no aerodynamic centre, and indeed $\bar{C}_M$, like the camber, is approximately proportional to α.

To determine the static stability of a sail aerofoil one must therefore examine the sign of x_{p2}, which is graphed in figure 6, along with the large-k asymptotic form. (The leading coefficient in the asymptotic form as $k \to k_c$ appears to be zero, so a more detailed analysis would be necessary to provide a formula.) It can be seen that x_{p2} is always positive (and the aerofoil always stable), but that x_{p2} decreases with increasing k.

4. Elastic sails and flexible structure (no slack)

Rigid structure

For a sail of no slack, attached to a rigid structure – i.e. to fixed leading and trailing edges – camber can be accommodated only by stretching the fabric. Let T be the sail tension with no airflow and T' the tension of the cambered sail. We assume a linear relation between T' and sail length:

$$l - c = \lambda_s(T' - T), \tag{4.1}$$

where

$$l = \int_0^c (1 + y'^2)^{\frac{1}{2}}\,\mathrm{d}x \tag{4.2}$$

is the sail length, and λ_s a constant coefficient of sail extensibility. From (4.1) and (4.2) we find

$$k' - k = \alpha^2 \Delta l / \Lambda_s, \tag{4.3}$$

where k' and k are the tension coefficients in the sail, with and without airflow,

$$\Delta l = \frac{1}{2c} \int_0^c y_1'^2 \, dx$$

is the α^2 coefficient of relative sail extension, and $\Lambda_s = \frac{1}{2}\rho U^2 \lambda_s$ is a dimensionless coefficient of sail extensibility. Equation (3.2) now becomes

$$C_L = \alpha C_{L1}(k') + \alpha^3 C_{L3}(k') + \ldots.$$

The coefficient C_{L1} can be expanded as a Taylor series about k to give

$$C_L = \alpha C_{L1}(k) + \alpha^3 \left[C_{L3}(k) + \Lambda_s^{-1} \Delta l \frac{dC_{L1}}{dk} \right] + O(\alpha^5), \tag{4.4}$$

and it follows similarly that

$$C_M = \alpha C_{M1}(k) + \alpha^3 \left[C_{M3}(k) + \Lambda_s^{-1} \Delta l \frac{dC_{M1}}{dk} \right] + O(\alpha^5), \tag{4.5}$$

and

$$x_p = x_{p0}(k) + \alpha^2 \left[x_{p2}(k) + \Lambda_s^{-1} \Delta l \frac{dx_{p0}}{dk} \right] + O(\alpha^5). \tag{4.6}$$

To leading order, the aerodynamic coefficients are independent of the sail elasticity, but increasing tension has the effect of somewhat reducing the terms of $O(\alpha^3)$, since the derivatives of the leading coefficients are all negative. If Λ_s is very small (and the sail almost inextensible) then these third-order corrections become important. Equation (4.6) shows that x_{p2} increases with Λ_s, and that there is a miminum value

$$\Lambda_s = \frac{\Delta l}{x_{p2}} \left| \frac{dx_{p0}}{dk} \right|$$

necessary to give stability.

Flexible structure

To model the structural flexibility of the trailing edge we suppose that its displacement $\boldsymbol{R}$ from the initial position $(c, 0)$ is a linear function of $\boldsymbol{f}$, the difference between the force exerted by the sail on the trailing edge and the initial force $-T\hat{\boldsymbol{x}}$. Thus we can write

$$R_i = A_{ij} f_j, \tag{4.7}$$

where A_{ij} is a constant 2×2 second-order tensor. We suppose $\boldsymbol{f}$ is conservative which implies A_{ij} is symmetric, and also that a force in the x-direction produces no y-displacement, so that the off-diagonal elements of A_{ij} must be zero. Then, referring to figure 7, one sees that (4.7) can be written in the form

$$c' \cos\beta - c = \lambda_x [T - T' \cos(\gamma' - \beta)], \tag{4.8}$$

$$c' \sin\beta = \lambda_y T' \sin(\gamma' - \beta), \tag{4.9}$$

where λ_x, λ_y are elastic constants.

The effective angle of incidence α' of the airflow to the aerofoil, whose chord has been rotated through an angle β by the trailing-edge displacement, is given by

$$\alpha' = \alpha - \beta. \tag{4.10}$$

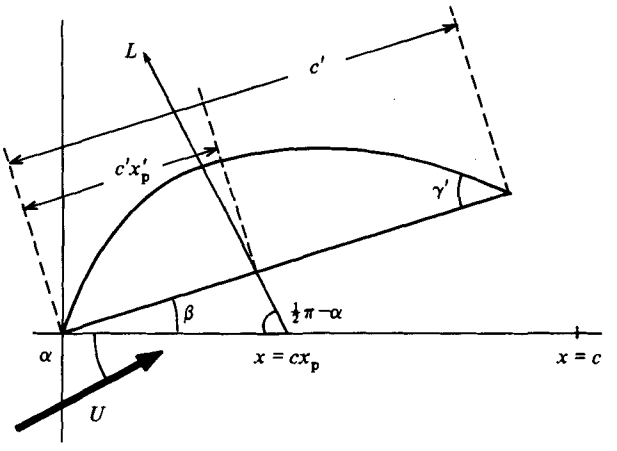

FIGURE 7. Diagram for analysing trailing-edge displacement.

The odd functions α', β and γ of α can be expanded as power series like (2.5), and the even functions c', k' in the form:

$$c' = c(1+\alpha^2 c_2+\ldots), \quad k' = k(1+\alpha^2 k_2+\ldots).$$

Equating terms of order α in (4.9) and (4.10) gives

$$\beta_1 = k\Lambda_y(\gamma_1\alpha_1'-\beta_1), \quad \alpha_1' = 1-\beta_1,$$

where $\Lambda_y = \frac{1}{2}\rho U^2\lambda_y$ is a dimensionless trailing-edge flexibility coefficient. It follows that

$$\beta_1 = \frac{\gamma_1 k\Lambda_y}{1+k\Lambda_y+\gamma_1 k\Lambda_y}, \quad \alpha_1' = \frac{1+k\Lambda_y}{1+k\Lambda_y+\gamma_1 k\Lambda_y}. \tag{4.11), (4.12}$$

The coefficient α_1' might be called the 'washout factor' – it gives the effective reduction in angle of attack due to the upward movement of the trailing edge. To within order α, the lift and moment coefficients will be reduced by multiplication by this same factor, which has a maximum value of 1 when $\Lambda_y = 0$ and decreases to a minimum of $1/(1+\gamma_1)$ as $\Lambda_y \to \infty$.

Static stability

Simple trigonometry applied to figure 7 gives

$$cx_p = c'x_p(k')(\cos\beta+\sin\beta\tan\alpha), \tag{4.13}$$

since $x_p' = x_p(k')$. When equating $O(\alpha^2)$ terms in this equation, it is necessary to expand $x_p(k')$ as a Taylor series in $k'-k$ to obtain

$$x_{p2} = x_{p0}(k)(c_2+\beta_1-\tfrac{1}{2}\beta_1^2)+\alpha_1'^2 x_{p2}(k)+kk_2\frac{dx_{p0}}{dk}. \tag{4.14}$$

Equating $O(\alpha^2)$ terms in (4.3) and (4.8) yields

$$k_2 = (k\Lambda_s)^{-1}(c_2+\alpha_1'^2\Delta l), \tag{4.15}$$

$$c_2-\tfrac{1}{2}\beta_1^2 = k\Lambda_x[\tfrac{1}{2}(\gamma_1\alpha_1'-\beta_1)^2-k_2]. \tag{4.16}$$

The variables k_2, c_2 can be found from (4.15) and (4.16) and substituted into (4.14)

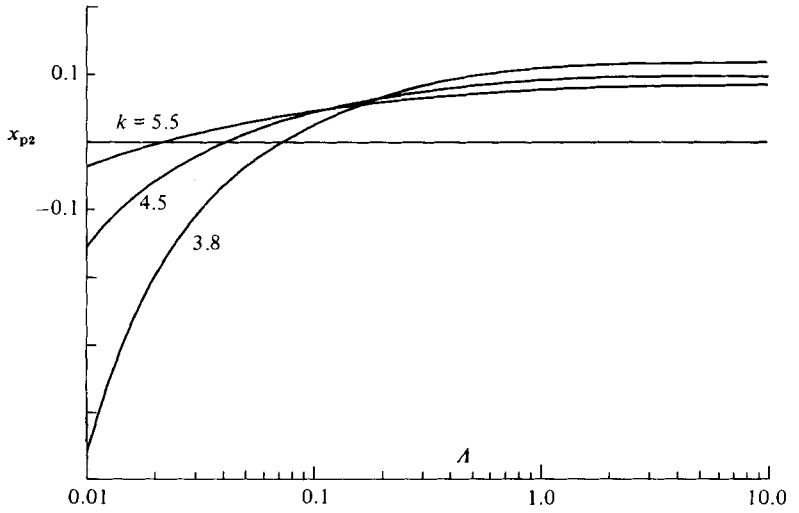

FIGURE 8. Effect of trailing-edge flexibility on longitudinal static stability.

to give a rather complicated formula for x_{p2}. To simplify matters we consider only the case of an inextensible sail ($\Lambda_s = 0$) and an isotropic trailing-edge structure so that $\Lambda_x = \Lambda_y = \Lambda$ say. Then we find

$$x_{p2} = x_{p0}\,(\tfrac{1}{2}-\tfrac{1}{2}\alpha_1'^2-\Delta l\alpha_1'^2)+\alpha_1'^2 x_{p2}(k)+\Lambda^{-1}[\tfrac{1}{2}\beta_1^2+\tfrac{1}{2}k\Lambda(\gamma_1\alpha_1'-\beta_1)^2+\Delta l\alpha_1'^2]\frac{\mathrm{d}x_{p0}}{\mathrm{d}k}. \tag{4.17}$$

Graphs of x_{p2} against Λ for various values of k are shown in figure 8. It appears that the stability increases with Λ, the main reason being that the effective decrease in α rotates the sail chord until it is more nearly perpendicular to the lift force, so increasing the moment about the leading edge.

5. Sails with slack

Section 4 dealt with sails that remained taut in still air, so that the camber tended to zero with α. Now consider a sail whose length under zero tension is $c(1+s)$, where s is a dimensionless slackness coefficient. We suppose that the sail is elastic with a coefficient of extensibility Λ_s (as defined in §4) and that the leading and trailing edges are fixed. When the sail is stretched under a tension corresponding to the smallest possible value k_c of k, its length will be $c(1+s)+c\Lambda_s k_c$, so we define s', the effective slack, by setting

$$s' = s+\Lambda_s k_c.$$

The theory in this section applies to any sail for which $s' > 0$. Thus a sail which is taut in still air, but under tension corresponding to $k = k_0$ say $< k_c$ will be considered as slack with $s' = \Lambda_s(k_c-k_0)$. Throughout this section we consider only the leading terms in the camber function and aerodynamic coefficients.

Coefficients when $\alpha \ll s'^{\frac{1}{2}}$

The sail camber αy_1 must be of order $s'^{\frac{1}{2}}$, so, if $\alpha \ll s'^{\frac{1}{2}}$, y_1 is large and $t = k-k_c$ must be small. The linear relation between sail tension and length gives

$$k\Lambda_s = \frac{l}{c}-(1+s) = \alpha^2\Delta l - s. \tag{5.1}$$

Substituting the small-t expansion of Δl from table 2 into (5.1) yields

$$t = \pm a^{\frac{1}{2}}\beta - \tfrac{1}{2}\beta^2(b + a\Lambda_s/s'), \tag{5.2}$$

where $a = 0.6718$, $b = 0.0859$ and the parameter β is as defined by Thwaites (1961):

$$\beta = \alpha/s'^{\frac{1}{2}}.$$

The existence of multiple solutions for k, corresponding to a small-enough fixed value of β, was noted by Thwaites (1961) (see his figure 6), and (5.2) in fact gives the two largest possible solutions, one $> k_c$ and the other $< k_c$. Haselgrove & Tuck (1976) showed that when $\Lambda_s = 0$ both of these solutions represent sails with profile stability, whereas all the other smaller solutions correspond to instability. The positive solution of (5.2) giving $k > k_c$ is the 'normal' one with the sail billowing to the lee, while the negative solution giving $k < k_c$ corresponds to a sail with 'reverse camber' – i.e. billowing to windward (but nonetheless having profile stability).

The lift coefficient can be estimated using (5.2) and the asymptotic form for C_{L1} given in table 2:

$$C_L \approx \pm 7.28 s'^{\frac{1}{2}} + \alpha(5.56 + 2.98\Lambda_s/s'). \tag{5.3}$$

Similar formulae can be derived for C_M and x_p:

$$C_M \approx \pm 3.12 s'^{\frac{1}{2}} + \alpha(0.95 + 1.49\Lambda_s/s'), \tag{5.4}$$

$$x_p \approx 0.5 - (\pm 0.28\alpha/s'^{\frac{1}{2}}). \tag{5.5}$$

Inextensible sails: $\alpha \gg s^{\frac{1}{2}}$

Consider now an inextensible sail with $\alpha \gg s^{\frac{1}{2}}$. Since the camber αy_1 must be of order $s^{\frac{1}{2}}$, y_1 must be small, and k large. Substituting the large-k asymptotic expansion for Δl into (5.1) gives

$$\frac{\alpha}{k} = \left[\frac{24s}{9\pi^2 - 64}\right]^{\frac{1}{2}}.$$

(Since now $\beta \gg 1$ there is only one solution.) The corresponding approximations to the aerodynamic coefficients are

$$C_L \approx (16 - \pi^2)\left[\frac{24}{9\pi^2 - 64}\right]^{\frac{1}{2}} s^{\frac{1}{2}} + 2\pi\alpha = 6.03 s^{\frac{1}{2}} + 2\pi\alpha, \tag{5.6}$$

$$C_M \approx \tfrac{1}{12}(64 - 3\pi^2)\left[\frac{24}{9\pi^2 - 64}\right]^{\frac{1}{2}} s^{\frac{1}{2}} + \tfrac{1}{2}\pi\alpha = 2.82 s^{\frac{1}{2}} + \tfrac{1}{2}\pi\alpha, \tag{5.7}$$

$$x_p \approx \tfrac{1}{4} + \frac{2}{3\pi}\left[\frac{24}{9\pi^2 - 64}\right]^{\frac{1}{2}} \frac{s^{\frac{1}{2}}}{\alpha} = \tfrac{1}{4} + 0.21\frac{s^{\frac{1}{2}}}{\alpha}. \tag{5.8}$$

The first term in (5.3) is identical with equation (30) of Nielsen (1963) for the lift coefficient when $\alpha = 0$. When the sail is elastic its camber increases more rapidly with α, which accounts for the presence of the term proportional to Λ_s. It is interesting to compare (5.3) and (5.6) with equation (72) of Thwaites (1961):

$$C_L = 6.36 s^{\frac{1}{2}} + 2\pi\alpha, \tag{5.9}$$

where $2\pi\alpha$ is the lift coefficient for a flat plate, and the coefficient 6.36 was chosen to fit, as closely as possible, a range of calculated values of C_L. Figure 9 compares the accuracy of the three formulae (for an inextensible sail). While (5.3) and (5.6) are more accurate than (5.9) in the appropriate α-limit, (5.9) is reasonably accurate over the

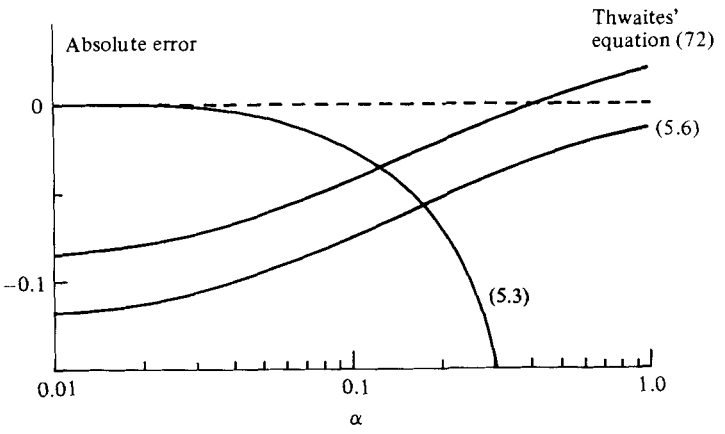

FIGURE 9. Comparison of errors involved in various approximations to C_L, for an inextensible sail, $s = 0.01$.

entire range of values of α. The different coefficients of α in (5.3) and (5.6) reflect different modes of camber variation in the two limits. As $\alpha \to 0$ and $k \to k_c$ the point of maximum camber approaches the midchord, since the sail profile is more and more dominated by $F(x)$. The symmetric profile is a more efficient lift generator, so the decrease in C_L as $\alpha \to 0$ is reduced. When $\alpha \gg s^{\frac{1}{2}}$, k is large and the sail profile almost constant, so the coefficient of α is just the flat-plate contribution, 2π. Equations (5.5) and (5.8) both show that sail aerofoils with slack are statically unstable, which is to be expected since they behave like rigid aerofoils, retaining finite camber as $\alpha \to 0$.

Flexible structure

Now suppose the trailing-edge displacement from its initial position $(c, 0)$ is given by (4.8) and (4.9). When $\alpha \ll s^{\frac{1}{2}}$ (5.2) can be substituted into the asymptotic form for γ_1 as $k \to k_c$ (table 2), and one finds

$$\gamma' \approx \gamma_1 \alpha' \approx 1.81 s'^{\frac{1}{2}}.$$

To leading order, (4.9) gives

$$\beta = k_c \Lambda_y (1.81 s'^{\frac{1}{2}} - \beta),$$

so that

$$\alpha' = \alpha - \beta = \alpha - \frac{1.81 s'^{\frac{1}{2}} k_c \Lambda_y}{1 + k_c \Lambda_y} \quad (\alpha \ll s^{\frac{1}{2}}). \tag{5.10}$$

Thus if

$$\alpha < \frac{1.81 s'^{\frac{1}{2}} k_c \Lambda_y}{1 + k_c \Lambda_y}$$

the effective angle of attack will become negative, the sail camber will reverse and the trailing edge move down again. Since no steady state can be achieved, the trailing edge will flap up and down.

The formula corresponding to (5.10) when $\alpha \gg s^{\frac{1}{2}}$ is

$$\alpha' = \alpha - \frac{\frac{1}{2}\pi \Lambda_y \alpha}{1 + \alpha \Lambda_y [(9\pi^2 - 64)/24s]^{\frac{1}{2}}}.$$

6. Discussion

The basic results of this paper are those described in §3 for a sail of constant tension coefficient k. These can be used to deduce the properties of elastic sails with or without slack, whose tension is initially unknown but can be determined from various forms of Hooke's law. The approximate analytic forms for the aerodynamic coefficients, summarized in table 2, are reasonably accurate over most ranges of k. In practice they would probably introduce less error than the assumption of laminar irrotational attached flow.

Sails without slack have the important property of neutral static stability (to leading order in α) and indeed, if they are sufficiently stretchable, they may have slight degree of positive stability. This property must be important in understanding the flight dynamics of bats and pterodactyls, whose wing consists of a tensioned elastic membrane without slack. Solid aerofoils (used by insects or birds) which acquire camber by bending under the influence of aerodynamic forces would have similar stability properties. Such an aerofoil with reverse camber in still air should be statically stable.

We have also seen that structural flexibility can have an important effect on the aerofoil characteristics. Sneyd *et al.* (1982) have analysed a model *Pteranodon* wing in which there is a spanwise variation in trailing-edge flexibility. This leads to a spanwise variation in the effective angle of attack – or an effective wing twist – which can give static stability. Another effect of a non-rigid trailing edge is to cause slack sails to flap at low angles of attack. This effect could be the cause of the dangerous fluttering nosedive which sometimes occurs in hang-glider flight.

An interesting feature of inextensible slack sails is the existence of two solutions when $\beta = \alpha/s^{\frac{1}{2}} \ll 1$, namely

$$y(x) \approx \pm 1.22 s^{\frac{1}{2}} F(x) + \alpha[G(x) + 0.064 F(x)]. \tag{6.1}$$

Haselgrove & Tuck (1976) showed that both of these solutions have profile stability, but argue that the sail will be unstable in this regime because it 'does not know' which of the two possible shapes to adopt. This is probably true in turbulent conditions, when large disturbances to the airflow could buffet the sail from one equilibrium to the other. In carefully controlled conditions the particular equilibrium adopted will depend on the way in which equilibrium is approached. For example if an initially positive angle of attack α is gradually reduced, the sail profile will follow (6.1) with the positive sign, and the corresponding tension will be given by (5.2) as

$$k = k_c + a^{\frac{1}{2}}\beta$$

to leading order in α. The sail profile and tension will continue to follow these formulae, even as α becomes negative, and the sail passes into 'reverse-camber' mode with $k < k_c$. Eventually if α is decreased until $\beta < 0.99$ the 'reverse-camber' solution no longer exists (see Thwaites 1961, figure 6), and the sail would flap across and billow to the lee in the normal way.

Strictly speaking, the work of Haselgrove & Tuck (1976) applies only to inextensible sails, and the profile-stability picture might be different if sail material or structural elasticity were taken into account.

Appendix A

Consider an inextensible surface S passing through two intersecting curves C_1, C_2. A coordinate system (u, v) can be constructed by drawing a network of lines over the surface, so that the equations of C_1 and C_2 are $v = 0$ and $u = 0$ respectively. Since the surface is inextensible, the length element $\mathrm{d}s$, given by

$$\mathrm{d}s^2 = E\,\mathrm{d}u^2 + 2F\,\mathrm{d}u\,\mathrm{d}v + G\,\mathrm{d}v^2,$$

is fixed, so E, F and G are prescribed functions of u and v over S. In particular, the surface area of S

$$\int_S (EG - F^2)^{\frac{1}{2}}\,\mathrm{d}u\,\mathrm{d}v$$

is fixed.

If $\boldsymbol{X}(u, v)$ denotes the position vector of the point on S with coordinates (u, v), the equation of C_1 is

$$\boldsymbol{x} = \boldsymbol{X}(u, 0).$$

Let $\hat{\boldsymbol{t}}$ and $\hat{\boldsymbol{n}}$ denote the unit tangent vector and principal normal to C_1, and κ the curvature. Then

$$\hat{\boldsymbol{t}} = E^{-\frac{1}{2}}\boldsymbol{X}_u$$

and

$$\begin{aligned}\kappa\hat{\boldsymbol{n}} &= E^{-\frac{1}{2}}\frac{\mathrm{d}}{\mathrm{d}u}(E^{-\frac{1}{2}}\boldsymbol{X}_u) = E^{-1}\boldsymbol{X}_{uu} - \tfrac{1}{2}E_u E^{-2}\boldsymbol{X}_u \\ &= E^{-1}(\Gamma^1_{11}\boldsymbol{X}_u + \Gamma^2_{11}\boldsymbol{X}_v + \alpha_{11}\hat{\boldsymbol{N}}) - \tfrac{1}{2}E_u E^{-2}\boldsymbol{X}_u. \qquad \text{(A 1)}\end{aligned}$$

The notation used is standard for differential geometry of surfaces (see e.g. Lipschutz 1969, equation (10.1)). Let $\hat{\boldsymbol{s}}$ be a unit vector lying in the surface and perpendicular to $\hat{\boldsymbol{t}}$:

$$\hat{\boldsymbol{s}} = (F\boldsymbol{X}_u - E\boldsymbol{X}_v)\,[E\,|EG - F^2|]^{-\frac{1}{2}}. \qquad \text{(A 2)}$$

Since the Γ-coefficients can be expressed in terms of E, F and G and their derivatives, it follows that $\kappa\hat{\boldsymbol{n}}\cdot\hat{\boldsymbol{s}}$ can be expressed likewise. Then the normal curvature of C_1,

$$\kappa_n = \kappa[1 - (\hat{\boldsymbol{n}}\cdot\hat{\boldsymbol{s}})^2]^{\frac{1}{2}} = \frac{L}{E}$$

(see Lipschutz 1969, p. 179), where L, M and N are the coefficients of the second fundamental form, can be evaluated along C_1, so L also is determined along C_1.

A similar argument shows that N is determined along C_2, and Gauss's Theorema Egregium proves that the Gaussian curvature $LN - M^2$, depending only on E, F, G and their derivatives, is known at every point of S. The Mainardi–Codazzi equations (Lipschutz 1969, equation (10.7)) provide a system of quasilinear partial differential equations for L and N. These equations are hyperbolic, since the lines of curvature are their characteristics, so the initial data prescribed on C_1 and C_2 will ensure a unique solution in some region bounded by the given curves. Thus the coefficients of both fundamental forms will be determined on some part S_0 of S, and the fundamental theorem of surfaces shows that this information determines S_0 uniquely, apart from a translation or rigid-body rotation.

Appendix B

The system of linear equations (2.21) for determining the array β_i of y' Fourier coefficients, can be written in the form

$$A_{0j}\beta_j = \beta_0, \tag{B 1}$$

$$A_{ij}\beta_j = c_i - \beta_0 A_{i0}, \quad i = 1, 2, \ldots, N, \tag{B 2}$$

where a repeated suffix implies summation from 1 to N. If X_i and Y_i are the solutions of

$$A_{ij}X_j = c_i, \quad A_{ij}Y_j = A_{i0}, \tag{B 3a, b}$$

it follows that

$$\beta_i = X_i - \beta_0 Y_i, \tag{B 4}$$

and then β_0 can be determined by substituting (B 4) into (B 1) to give

$$\beta_0 = \frac{A_{0j}X_j}{1 + A_{0j}Y_j}. \tag{B 5}$$

The reduced $N \times N$ matrix A_{ij} is real and symmetric, and has real eigenvalues (in ascending order) $\lambda_1, \lambda_2, \ldots, \lambda_N$ with corresponding real orthogonal unit eigenvectors $e_{1i}, e_{2i}, \ldots, e_{Ni}$ say. Equations (B 3a) can be solved in terms of the eigenvectors:

$$\begin{aligned} X_i &= c_j e_{pj} e_{pi}/\lambda_p \\ &= c_j e_{1j} e_{1i}/\lambda_1 + x_i \end{aligned}$$

say. As $k - k_c = t$ say $\to 0$, $\lambda_1 \to 0$, so for small t we can write

$$X_i = X_{i1}t^{-1} + X_{i0} + O(t), \tag{B 6}$$

where

$$X_{i1} = c_j e_{1j} e_{1i}/\lambda_1' \tag{B 7}$$

and

$$X_{i0} = x_i + c_j(e_{1j}' e_{1i} + e_{1j} e_{1i}')/\lambda_1' - c_j e_{1j} e_{1i} \lambda_1''/\lambda_1'^2, \tag{B 8}$$

where λ_1' denotes $(\mathrm{d}\lambda_1/\mathrm{d}k)_{k=k_c}$ etc. A similar expansion

$$Y_i = Y_{i1}t^{-1} + Y_{i0} + O(t) \tag{B 9}$$

can also be found. When β_0 is calculated from (B 5), no terms of order t^{-1} will appear since both X_{i1} and Y_{i1} are proportional to e_{1i}, whose even components are all zero, so that $A_{0j}e_{1j} = 0$.

From (B 4), (B 6) and (B 9) it can be seen that $F(x)$ in (3.1) is determined by the requirement that $F'(x)$ have Fourier coefficients $X_{i1} - \beta_0 Y_{i1}$. The function $G(x)$ is similarly determined from $X_{i0} - \beta_0 Y_{i0}$.

The array of $F'(x)$ Fourier coefficients is proportional to e_{1i}, so the even coefficients are all zero. This means that $F(x)$ is symmetric about $\theta = \frac{1}{2}\pi$ – the midchord of the aerofoil.

REFERENCES

Bundock, M. S. 1980 M.Sc. dissertation, University of Waikato.

Chalmers, L. G. 1966 *Q. J. Mech. Appl. Maths* **19**, 221–231.

Haselgrove, M. K. & Tuck, E. O. 1976 Stability properties of the two-dimensional sail model. In *New England Sailing Yacht Symp. Proc.* Soc. Naval Arch. and Mar. Engrs, New York.

Lipschutz, M. M. 1969 *Theory and Problems of Differential Geometry.* McGraw-Hill.

NIELSEN, J. N. 1963 *Trans. ASME* E: *J. Appl. Mech.* **30**, 435–442.
SNEYD, A. D., BUNDOCK, M. S. & REID, D. F. 1982 *Am. Naturalist* **120**, 455–477.
THWAITES, B. 1961 *Proc. R. Soc. Lond.* A **261**, 402–422.
VANDEN-BROECK, J.-M. 1982 *Phys. Fluids* **25**, 420–423.
VANDEN-BROECK, J.-M. & KELLER, J. B. 1981 *Phys. Fluids* **24**, 552–555.